RESEARCH ARTICLE | FEBRUARY 02 2023

Molecular beam epitaxy of $KTaO_3$

Special Collection: Thin Film Deposition for Materials Discovery

Tobias Schwaigert ; Salva Salmani-Rezaie ; Matthew R. Barone ; Hanjong Paik ; Ethan Ray ; Michael D. Williams ; David A. Muller ; Darrell G. Schlom ; Kaveh Ahadi

Journal of Vacuum Science & Technology A 41, 022703 (2023)
https://doi.org/10.1116/6.0002223

JVST A
Journal of Vacuum Science & Technology A

ARTICLE

avs.scitation.org/journal/jva

Molecular beam epitaxy of $KTaO_3$

Cite as: J. Vac. Sci. Technol. A 41, 022703 (2023); doi: 10.1116/6.0002223
Submitted: 14 September 2022 · Accepted: 20 December 2022 ·
Published Online: 2 February 2023

Tobias Schwaigert,[1,2] Salva Salmani-Rezaie,[3,4] Matthew R. Barone,[1,2] Hanjong Paik,[1,5,6] Ethan Ray,[1] Michael D. Williams,[7] David A. Muller,[3,4] Darrell G. Schlom,[1,2,4,8] and Kaveh Ahadi[9,10,a)]

AFFILIATIONS

[1]Platform for the Accelerated Realization, Analysis, and Discovery of Interface Materials (PARADIM), Cornell University, Ithaca, New York 14853
[2]Department of Materials Science and Engineering, Cornell University, Ithaca New York 14853
[3]School of Applied and Engineering Physics, Cornell University, Ithaca, New York 14853
[4]Kavli Institute at Cornell for Nanoscale Science, Cornell University, Ithaca, New York 14853
[5]School of Electrical & Computer Engineering, University of Oklahoma, Norman, Oklahoma 73019
[6]Center for Quantum Research and Technology, University of Oklahoma, Norman, Oklahoma 73019
[7]Department of Physics, Clark Atlanta University, Atlanta, Georgia 30314
[8]Leibniz-Institut für Kristallzüchtung, Max-Born-Str. 2, 12489 Berlin, Germany
[9]Department of Materials Science and Engineering, North Carolina State University, Raleigh, North Carolina 27265
[10]Department of Physics, North Carolina State University, Raleigh, North Carolina 27695

Note: This paper is a part of the Special Topic Collection on Thin Film Deposition for Materials Discovery.

[a)]**Electronic mail:** kahadi@ncsu.edu

ABSTRACT

Strain-engineering is a powerful means to tune the polar, structural, and electronic instabilities of incipient ferroelectrics. $KTaO_3$ is near a polar instability and shows anisotropic superconductivity in electron-doped samples. Here, we demonstrate growth of high-quality $KTaO_3$ thin films by molecular-beam epitaxy. Tantalum was provided by either a suboxide source emanating a TaO_2 flux from Ta_2O_5 contained in a conventional effusion cell or an electron-beam-heated tantalum source. Excess potassium and a combination of ozone and oxygen (10% O_3 + 90% O_2) were simultaneously supplied with the TaO_2 (or tantalum) molecular beams to grow the $KTaO_3$ films. Laue fringes suggest that the films are smooth with an abrupt film/substrate interface. Cross-sectional scanning transmission electron microscopy does not show any extended defects and confirms that the films have an atomically abrupt interface with the substrate. Atomic force microscopy reveals atomic steps at the surface of the grown films. Reciprocal space mapping demonstrates that the films, when sufficiently thin, are coherently strained to the $SrTiO_3$ (001) and $GdScO_3$ (110) substrates.

I. INTRODUCTION

Complex transition metal oxides exhibit a broad spectrum of orders and instabilities. Tuning the rich and often record properties of these materials is facilitated by their incorporation in high-quality epitaxial heterostructures where strain, juxtaposed competing orders, or other methodologies to modify the ground state can be imposed.[1–4] $KTaO_3$ is an incipient ferroelectric, in which superconductivity emerges at low temperatures in electron-doped samples.[5–7] The $KTaO_3$ conduction band is derived from the Ta 5*d* states and shows highly anisotropic electronic transport.[8–10] Furthermore, charge carriers in $KTaO_3$ have smaller effective mass and larger spin–orbit coupling compared to $SrTiO_3$.[11,12] These opportunities invite the intensive study of $KTaO_3$-based thin films and heterostructures to understand and engineer these phenomena. Surprising, the growth of $KTaO_3$ by molecular-beam epitaxy (MBE) has not been demonstrated.

The main challenges to the MBE growth of $KTaO_3$ are to provide a stable tantalum flux and the high chemical reactivity between potassium metal and air that complicates the use of elemental potassium as an MBE source. Tantalum is a refractory metal, requiring temperatures in excess of 2600 °C to evaporate at typical oxide MBE growth rates.[13] Successful MBE growth of tantalates remains elusive and has been limited to the use of electron-beam

(e-beam) evaporator sources to reach the temperatures needed to evaporate elemental tantalum. This approach has been used to grow $LiTaO_3$[14] and more recently Ta_2SnO6.[15] Recent thermodynamic calculations, however, suggest Ta_2O_5 as a potential source for the MBE growth of tantalates that can be accomplished at temperatures attainable in an MBE effusion cell.[16] Elemental potassium is highly reactive and readily oxidizes in air. A means to circumvent this issue is through the preparation of intermetallic compounds of alkali metals in a glovebox with relatively low vapor pressure elements, e.g., $LiSn_4$ and $CsIn_3$, as have been recently explored as MBE sources.[17,18]

Here, we demonstrate the MBE growth of high-quality $KTaO_3$ films using either traditional elemental tantalum in an e-beam evaporator or a Ta_2O_5 source contained in a high-temperature MBE effusion cell. Potassium was evaporated from an In_4K intermetallic compound source. A combination of ozone and oxygen (10% O_3 + 90% O_2) was used as the oxidant. The structural quality of the epitaxial $KTaO_3$ films grown in multiple strain states was assessed using a wide range of characterization techniques. Although we have grown roughly fifty $KTaO_3$ films with comparable quality, only the best three samples are featured in this article.

II. EXPERIMENT

Epitaxial $KTaO_3$ films were grown in a Vecco GEN 10 MBE system. A molecular beam of TaO_2 (gas) flux was generated from an effusion cell containing Ta_2O_5 (Alfa Aesar, 99.993%) contained in an iridium crucible. The suboxide TaO_2 is the most volatile species in the growth temperature range.[16] Potassium was evaporated from an effusion cell, containing intermetallic In_4K, which melts at elevated temperatures compared to pure potassium (432 °C vs 63.5 °C), improving the temperature control and flux stability.[19] The K-In alloy was prepared in a glovebox and contained in a titanium crucible. Once prepared, it can be exposed to air, facilitating its handling and loading. The vapor pressure of potassium is more than 10^{10} times higher than indium at the K-In cell temperature of 300–400 °C.[13] $GdScO_3$ $(110)_o$ (Crystec GmbH) substrates were used as received and the $SrTiO_3$ (001) substrates were terminated following the procedure developed by Koster *et al.*[20] Films were grown by codeposition of potassium, TaO_2 (or tantalum), and ozone at a substrate temperature of 625 °C as measured by an optical pyrometer operating at a wavelength of 1550 nm. The pyrometer measures the temperature of the platinum coating that has been evaporated on the backside of the substrate to facilitate radiative heat transfer from the SiC heating element of the MBE system to the substrate. The K:Ta flux ratio was kept at approximately 10:1. A mixture of ozone and oxygen (10% O_3 + 90% O_2) was used as the oxidant. The films were grown at an oxidant background pressure of 1×10^{-6} Torr. Typical fluxes for the sources were $(4–7)\times10^{12}$ atoms/cm^2/s for TaO_2 and $(4–7)\times10^{13}$ atoms/cm^2/s for potassium, determined by a quartz crystal microbalance (QCM), with an accuracy of about ±15%. In a typical growth experiment, the potassium flux was measured first, followed by TaO_2 to ensure that the QCM was as close to RT as possible for the most accurate reading. For a more detailed description, the reader is referred to the supplementary material.[21] Codeposition with these fluxes results in a $KTaO_3$ film growth rate of about 0.03 Å/s.

X-ray diffraction (XRD), x-ray reflectometry (XRR), and reciprocal space mapping (RSM) measurements were carried out using a PANalytical Empyrean diffractometer with Cu $K\alpha_1$ radiation. The raw XRR spectra were analyzed using the PANalytical X'Pert Reflectivity software package and the layer thickness was derived from a fast Fourier transform (FFT) after manually defining the critical angle to account for refractive effects. *In situ* reflection high-energy electron diffraction (RHEED) patterns were recorded using KSA-400 software and a Staib electron source operated at 14 kV and a filament current of 1.5 A. The morphology of the film surface was characterized using an Asylum Cypher ES environmental AFM. Cross-sectional scanning transmission electron microscopy (STEM) samples were prepared using a standard lift-out process using a Thermo Fisher Scientific Helios G4UX focused ion beam with the final milling voltage of 2 kV for the gallium ions. A Thermo Fisher Scientific Spectra 300 X-CFEG, operating at 200 kV with a convergence angle of 30 mrad and a high-angle annular dark-field (HAADF) detector with an angular range of 60–200 mrad, was used to collect atomic resolution HAADF-STEM images. STEM energy-dispersive x-ray spectroscopy (EDX) data were collected using a steradian Dual-X EDX detector with a probe current of 100 pA. The noise of the STEM-EDX spectrum was reduced by the application of principal component analysis.

III. RESULTS

$KTaO_3$ is a cubic perovskite with a lattice constant of $a_{KTO} = 3.988$ Å[22] at room temperature. The lattice mismatch between $KTaO_3$ and $GdScO_3$ (pseudo-cubic lattice-constant, 3.967 Å[23]) and $SrTiO_3$ ($a_{STO} = 3.905$ Å[24]) are −0.5% and −2.1%, respectively. $KTaO_3$ grows "cube-on-cube" on $SrTiO_3$ (001) substrates and "cube-on-pseudocube" on $GdScO_3$ $(110)_o$ substrates. Reflection high-energy electron diffraction (RHEED) was used to monitor the evolution of the surface structure and reconstruction during growth. Figures 1(a) and 1(b) show the $GdScO_3$ $(110)_o$ substrate along the high symmetry directions where diffraction streaks and Kikuchi lines are visible. Figures 1(c) and 1(d) show the diffraction pattern 1 min after the start of the growth (corresponding to the deposition of a $KTaO_3$ film about one half of a unit cell thick on average) using the suboxide source. Kikuchi lines are still visible, but the diffraction pattern has evolved to $KTaO_3$ (001). The RHEED pattern appears cloudy, suggesting a floating potassium oxide layer. The films are grown in a K-rich regime with a K:Ta flux ratio of 10:1 within an absorption-controlled growth regime exploiting the volatility of the potassium oxide species on the growth surface. Deviation from this flux ratio increases the roughness of the films. Figures 1(e) and 1(f) show the $KTaO_3$ RHEED streaks immediately after the growth of an 18 nm thick $KTaO_3$ film, where the shutters of the TaO_2 and potassium sources have been closed, but the substrate is still immersed in ozone and beginning to be cooled down from the growth temperature. Atomic force microscopy (AFM) images are shown in Figs. 1(g) and 1(h) at different magnifications. Atomic steps from the <0.05° off-cut substrate are visible. The root-mean-square (rms) roughness for Fig. 1(h) is ≈640 pm, measured by taking a 1 μm^2 area as a reference.

Figure 2 shows the x-ray diffraction results of the same 18 nm thick $KTaO_3$ film grown on a $GdScO_3$ $(110)_o$ substrate using the suboxide source. The film thickness is calculated using the Laue fringes and corroborated with x-ray reflectivity and cross-sectional HAADF-STEM. The θ-2θ XRD scan only shows 00ℓ peaks,

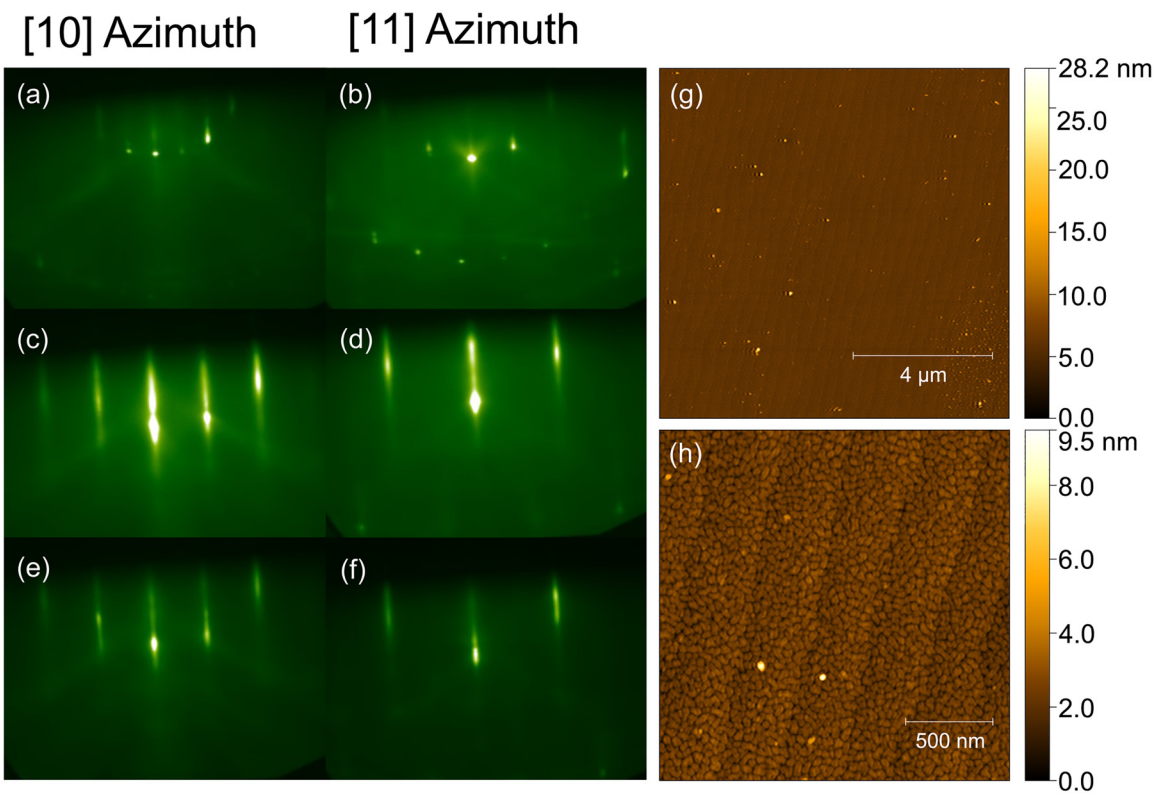

FIG. 1. RHEED patterns of (a) and (b) bare $GdScO_3$ substrate; (c) and (d) after 1 min (approximately 0.5 unit cell average thickness) $KTaO_3$ growth; and (e) and (f) immediately after the growth of an 18 nm thick $KTaO_3$ film with an effusion cell containing Ta_2O_5. (g) and (h) Atomic force microscopy images at different magnifications, revealing atomic steps.

confirming that the film is single-phase and oriented with its c-axis perpendicular to the plane of the substrate. Figure 2(b) depicts a close-up θ-2θ scan around the $KTaO_3$ 001 peak, showing symmetric Laue fringes. The rocking curve full width at half maximum (FWHM) of the $KTaO_3$ film is comparable to the $GdScO_3$ substrate (both about 30 and 60 arcsec, respectively, along the two orthogonal in-plane directions of the substrate), suggesting the high crystalline quality of the grown films. X-ray reciprocal space mapping (RSM) around the $GdScO_3$ 332 and $KTaO_3$ 103 reflections confirms that the film is coherently strained to the substrate.

We apply elasticity theory to see how the observed out-of-plane lattice spacing of a commensurately strained $KTaO_3$ film grown on $SrTiO_3$ compares to a calculation using the elastic stiffness tensor of $KTaO_3$.[25] The out-of-plane lattice $a_\perp$ can be calculated from the out-of-plane strain, $\epsilon_{33} = \frac{(a_\perp - a_{KTO})}{a_{KTO}}$ by expanding the tensor equation (in Einstein notation): $\sigma_{ij} = c_{ijkl}\epsilon_{kl}$ for σ_{33} and recognizing that $\sigma_{33} = 0$ because the film is free of stress in the out-of-plane direction. This leads to

$$a_\perp = a_{KTO} + \frac{2(a_{KTO} - a_{STO})c_{12}}{c_{11}}, \quad (1)$$

where c_{11} and c_{12} are elastic stiffness tensor coefficients of $KTaO_3$ in Voigt notation and a_{KTO} and a_{STO} are the lattice constants of unstrained $KTaO_3$ and $SrTiO_3$, respectively. The calculated out-of-plane lattice constant expected for a commensurately strained $KTaO_3$ film on $SrTiO_3$ at room temperature is 4.028 Å. This is lower than the 4.043 ± 0.015 Å value measured by x-ray diffraction for the commensurately strained 10.5 nm thick $KTaO_3$ film shown in Figs. S1 and S2[21] (which was grown using an elemental tantalum molecular beam).

In contrast to the extended out-of-plane lattice spacing observed for the commensurately strained $KTaO_3$ film grown on a $SrTiO_3$ substrate, the 18 nm thick commensurately strained $KTaO_3$/$GdScO_3$ shown in Figs. 1–3 shows the expected out-of-plane spacing, calculated with the elastic theory. Because $GdScO_3$ is orthorhombic, the in-plane biaxial strains ϵ_{11} and ϵ_{22} imposed by the substrate are no longer equal and the equation for $a_\perp$ becomes

$$a_\perp = a_{KTO} + \frac{(4a_{KTO} - a_{GSO_{001}} - a_{GSO_{1\bar{1}0}})c_{12}}{2c_{11}}, \quad (2)$$

where $a_{GSO_{001}}$ and $a_{GSO_{1\bar{1}0}}$ are the in-plane distances that establish ϵ_{11} and ϵ_{22} through commensurate strain. Specifically, $a_{GSO_{001}}$ is the

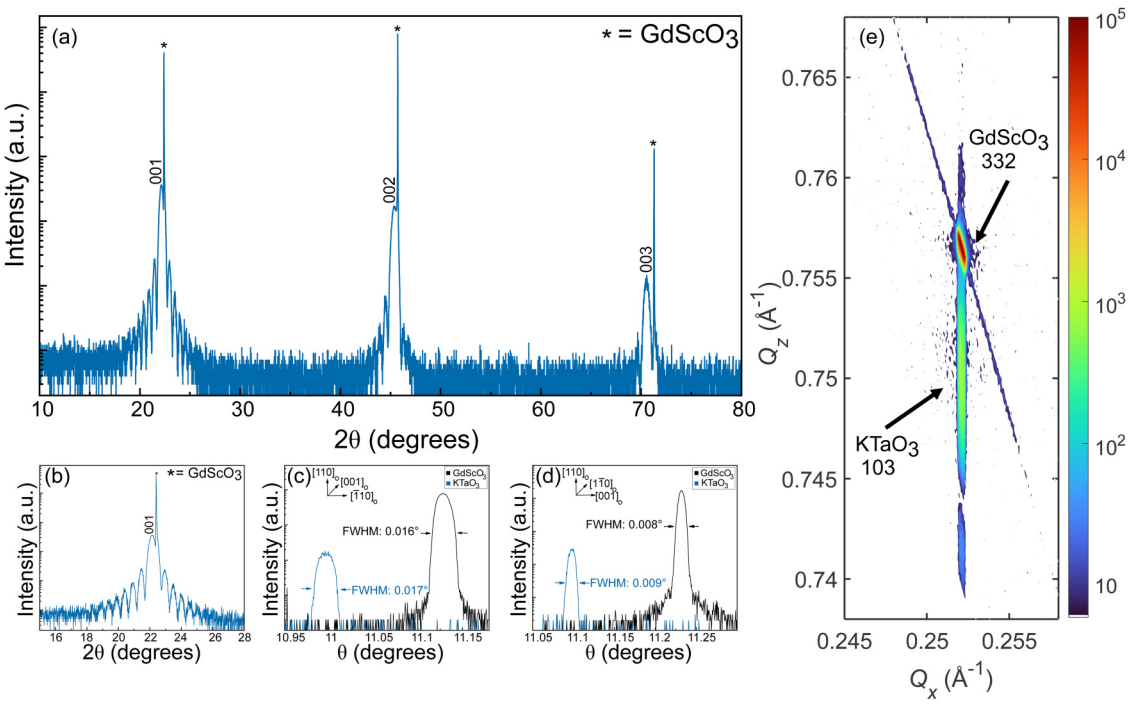

FIG. 2. X-ray diffraction of the 18 nm thick $KTaO_3$ film grown on a $GdScO_3$ $(110)_o$ substrate with an effusion cell containing Ta_2O_5 . (a) θ-2θ scan, showing 00ℓ peaks of $KTaO_3$. Symmetric Laue fringes indicate a well-defined film thickness, indicative of an abrupt interface between film and substrate (asterisks * denote substrate reflections). (b) A zoomed-in θ-2θ scan in the vicinity of the $KTaO_3$ 001 peak, showing the Laue fringes used to calculate the film thickness. (c) and (d) Overlaid rocking curves of the 110 $GdScO_3$ and 001 $KTaO_3$ peaks, showing comparable FWHMs, indicating low out-of-plane mosaicity ($\Delta\omega \approx 0.017°$ and 0.008° along the two orthogonal in-plane directions of the substrate). (e) reciprocal space map (RSM) around the 332 substrate and 103 film reflections. The RSM results confirm that the film is fully strained to the substrate.

c axis length of $GdScO_3$ (7.9314 Å) and $a_{GSO_{1\bar{1}0}}$ is the $[1\bar{1}0]$ length of $GdScO_3$ (7.9401 Å),[26] where we are using the nonstandard *Pbnm* setting of $GdScO_3$ as is most common in the literature. Here, the calculations result in an expected spacing of 3.998 Å at room temperature compared to the 3.997 ± 0.01 Å measured by x-ray diffraction.

The films grown in $GdScO_3$ do not show any discrepancy between the measured and the calculated out-of-plane lattice parameter. Interestingly, $KTaO_3$ films grown on $SrTiO_3$ do show a discrepancy between the measured and calculated out-of-plane lattice parameter, which could be explained by the emergence of a ferroelectric state in films grown on $SrTiO_3$. Another possible explanation could be that the film grown on $SrTiO_3$ might be non-stoichiometric. Errors in stoichiometry are known to lengthen the lattice constants of many perovskites, e.g., $SrTiO_3$,[27,28] $CaTiO_3$,[29] and $SrVO_3$,[30] but in other cases, e.g., $LaVO_3$,[31] can shorten them. The samples shown here are grown in an absorption controlled growth regime, yielding phase-pure $KTaO_3$. Nonetheless, phase purity is not synonymous with a stoichiometric $KTaO_3$ film and it is possible that the growth conditions we have employed lead to non-stoichiometric $KTaO_3$ films. If it is due to non-stoichiometry, the significant lattice expansion observed might be expected to give rise to extended defects as is the case for Sr-rich $SrTiO_3$ films.[27] Low-magnification HAADF-STEM, however, does not show any extended defects in these films and can be found in the supplementary material in Fig. S7.[21] A more interesting possibility is that the lattice expansion is intrinsic and is due to the $KTaO_3$ under biaxial compression becoming ferroelectric with an out-of-plane polarization. For the $KTaO_3/SrTiO_3$ system, first-principles calculations find that biaxial compressive strains of magnitude larger than 1% are needed to induce ferroelectricity.[32] This could elongate the out-of-plane lattice constant beyond that expected from an elasticity calculation because the ground state has changed from paraelectric $KTaO_3$ to ferroelectric $KTaO_3$ for the film commensurately strained to $SrTiO_3$ (−2.1% strain), but not when $KTaO_3$ is grown on $GdScO_3$ (−0.5% strain). Future studies are planned to investigate this possibility.

Figure S1[21] compares the XRD of the $KTaO_3$ films grown using a TaO_2 suboxide molecular beam and a tantalum molecular beam from an e-beam-heated elemental tantalum source. Both $KTaO_3$ films were grown on $SrTiO_3$ (001) substrates at similar substrate temperature and ozone partial pressure. Figures S2 and S3[21] show the x-ray diffraction θ-2θ scans, RSM, and AFM characterization of these same films grown using suboxide and tantalum e-beam sources. Interestingly, the $KTaO_3$ film, using the tantalum e-beam source, is strained to the $SrTiO_3$ (001) substrate. This is

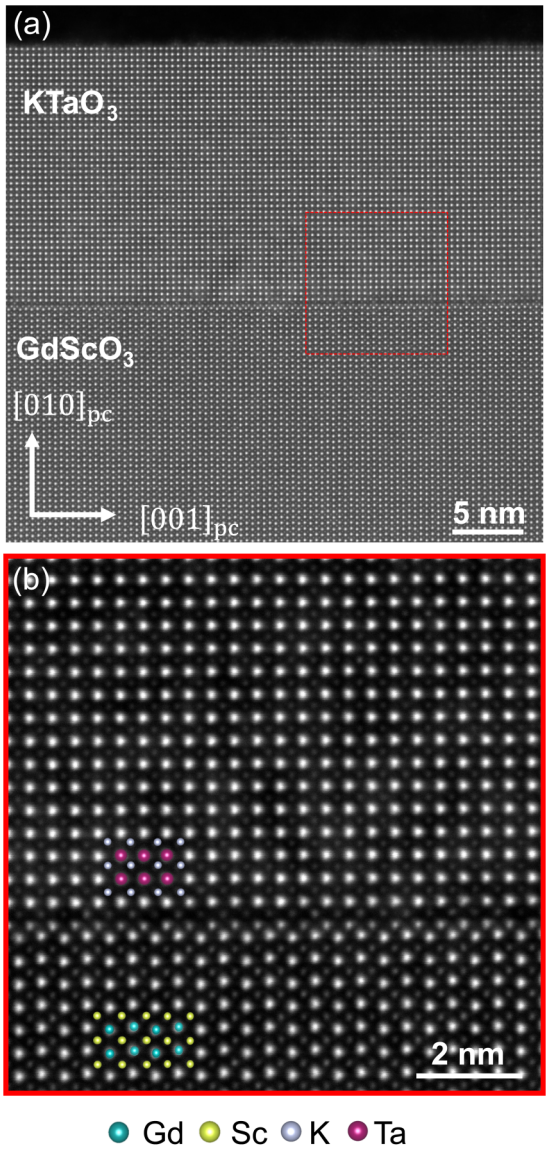

FIG. 3. (a) Cross-sectional HAADF-STEM images of the same 18 nm thick $KTaO_3$ film grown on a $GdScO_3$(110) substrate with an effusion cell containing Ta_2O_5. (b) Higher magnification HAADF-STEM image of the $KTaO_3/GdScO_3$ interface showing the bilayer of the intermixed metal ions.

noteworthy due to the large lattice mismatch between $KTaO_3$ and $SrTiO_3$ ($\approx -2.1\%$). The surface morphology revealed by AFM shows a smoother surface for the e-beam film. The AFM image of the suboxide film shows potassium oxide (K_2O) residues on the surface. This could be due to the presence of additional oxygen which oxidizes the potassium atoms, leading to a higher sticking coefficient. The rms roughness of the e-beam film is ≈0.3 nm compared to ≈1.8 nm for the suboxide film. The RSM around the $SrTiO_3$ and $KTaO_3$ 103 peak shows that only the e-beam sample is commensurately strained and the suboxide film is partially relaxed. The difference could be simply due to the difference in thickness: 22.5 and 10.5 nm for the suboxide and e-beam films, respectively. It is important to point out that an equivalent surface roughness can be achieved with the suboxide source and in thicker films (See Fig. 1).The initial results showed rougher surfaces with suboxide sources. After fine-tuning the growth parameters, we find that the suboxide sources also produce films that are atomically flat similar to those produced with the tantalum e-beam source. The flux emanating from the Ta_2O_5 source is not only far more stable than the flux produced by the tantalum e-beam source, but the suboxide flux can be increased to produce growth rates up to 100 nm/h. For these reasons, we find the Ta_2O_5 source preferable for the growth of $KTaO_3$ films by MBE.

A high-angle annular dark-field scanning transmission electron microscope (HAADF-STEM) was used to further investigate the $KTaO_3$ films. The HAADF-STEM image along the $GdScO_3[100]_{pc}$ zone axis (Fig. 3), where the subscript *pc* denotes pseudocubic indices, shows a coherent epitaxial interface between the $KTaO_3$ film and underlying $GdScO_3$ substrate. $KTaO_3$ and $GdScO_3$ both have polar surfaces and the formation of two layers of intermixed metal ions can relieve the polar catastrophe at the interface. Figure 3(b) shows that the interface has the proposed[33] bilayer structure with $K_xGd_{1-x}O$(top)/$Ta_ySc_{1-y}O_2$(bottom) to relieve the polarity conflict of the $KTaO_3$ and $GdScO_3$ interface. STEM-EDX analysis of the interface (Fig. S5[21]) and the intensity line profile of the HAADF-STEM images (Fig. S6[21]) also point to the formation of the intermixed bilayer structure.

In summary, we demonstrate the MBE growth of high-quality $KTaO_3$ films. Suboxide and tantalum e-beam sources are used and compared. Potassium, evaporated from an In_4K compound source, provides reasonable flux stability. Symmetric Laue fringes suggest that the films are smooth. Cross-sectional HAADF-STEM does not show any extended defects and reveals an atomically abrupt film/substrate interface. RSM confirms that when sufficiently thin the films are coherently strained to the substrates. The repeatability of the results and observed lattice spacings that are consistent with the stoichiometric growth of $KTaO_3$ for strains where ferroelectricity is not expected, i.e., $KTaO_3/GdScO_3$ (110), suggest that the growth by codeposition occurs in an absorption-controlled regime.

ACKNOWLEDGMENTS

This work made use of the synthesis and electron microscopy facilities of the Platform for the Accelerated Realization, Analysis, and Discovery of Interface Materials (PARADIM), which are supported by the National Science Foundation under Cooperative Agreement No. DMR-2039380. M.D.W., D.A.M., and D.G.S acknowledge support from the National Science Foundation (NSF) under No. DMR-2122147. This work made use of the Cornell Center for Materials Research (CCMR) Shared Facilities, which are supported through the NSF MRSEC Program No. DMR-1719875. This work made use of a Helios FIB supported by NSF (Grant No. DMR-1539918) and the Cornell Center for Materials Research (CCMR) Shared Facilities, which are supported through the NSF MRSEC Program (Grant No. DMR-1719875). K.A. acknowledges conversation with Zlatko Sitar. The authors acknowledge Steve

Button for substrate preparation. The authors gratefully acknowledge Nicholas A. Parker and Yilin Evan Li for help with the AFM experiment, Sankalpa Hazra and Tatiana Kuznetsova for growing the sample used for SIMS experiment, and Dasol Yoon and Xiyue Zhang for providing EDX analysis code. M.D.W. also acknowledges NSD HRD1924204.

AUTHOR DECLARATIONS

Conflict of Interest

The authors have no conflicts to disclose.

Author Contributions

Tobias Schwaigert: Data curation (equal); Formal analysis (equal); Investigation (equal); Methodology (equal); Visualization (lead); Writing – original draft (lead); Writing – review & editing (lead). **Salva Salmani-Rezaie:** Data curation (equal); Formal analysis (equal); Investigation (equal); Visualization (equal); Writing – review & editing (equal). **Matthew R. Barone:** Formal analysis (equal); Investigation (equal); Validation (equal). **Hanjong Paik:** Formal analysis (equal); Investigation (equal); Validation (equal). **Ethan Ray:** Investigation (supporting). **Michael D. Williams:** Data curation (equal); Formal analysis (equal); Investigation (supporting); Validation (supporting). **David A. Muller:** Formal analysis (equal); Investigation (equal); Visualization (equal). **Darrell G. Schlom:** Formal analysis (equal); Investigation (equal); Methodology (equal); Supervision (equal); Validation (equal); Writing – review & editing (equal). **Kaveh Ahadi:** Conceptualization (lead); Formal analysis (equal); Investigation (equal); Methodology (equal); Supervision (equal); Validation (equal); Writing – original draft (equal); Writing – review & editing (equal).

DATA AVAILABILITY

The data that support the findings of this study are available within the article. Additional data related to the film growth and structural characterization by XRD and STEM are available at https://doi.org/10.34863/crr6-z966. Any additional data connected to the study are available from the corresponding author upon reasonable request.

REFERENCES

[1]J. H. Haeni *et al.* , Nature **430**, 758 (2004).
[2]K. Ahadi, L. Galletti, Y. Li, S. Salmani-Rezaie, W. Wu, and S. Stemmer, Sci. Adv. **5**, eaaw0120 (2019).
[3]J. H. Lee *et al.* , Nature **466**, 954 (2010).
[4]K. Ahadi, L. Galletti, and S. Stemmer, Appl. Phys. Lett. **111**, 172403 (2017).
[5]K. Ueno, S. Nakamura, H. Shimotani, H. Yuan, N. Kimura, T. Nojima, H. Aoki, Y. Iwasa, and M. Kawasaki, Nat. Nanotechnol. **6**, 408 (2011).
[6]C. Liu *et al.*, Science **371**, 716 (2021).
[7]A. Gupta, H. Silotia, A. Kumari, M. Dumen, S. Goyal, R. Tomar, N. Wadehra, P. Ayyub, and S. Chakraverty, Adv. Mater. **34**, 2106481 (2022).
[8]A. H. Al-Tawhid, D. P. Kumah, and K. Ahadi, Appl. Phys. Lett. **118**, 192905 (2021).
[9]A. H. Al-Tawhid, J. Kanter, M. Hatefipour, D. L. Irving, D. P. Kumah, J. Shabani, and K. Ahadi, J. Electron. Mater. **51**, 7073 (2022).
[10]A. H. Al-Tawhid, J. Kanter, M. Hatefipour, D. P. Kumah, J. Shabani, and K. Ahadi, J. Electron. Mater. **51**, 6305 (2022).
[11]H. Nakamura and T. Kimura, Phys. Rev. B **80**, 121308 (2009).
[12]N. Wadehra, R. Tomar, R. M. Varma, R. Gopal, Y. Singh, S. Dattagupta, and S. Chakraverty, Nat. Commun. **11**, 1 (2020).
[13]R. Honig and D. A. Kramer, RCA Rev. **30**, 285 (1969).
[14]F. Gitmans, Z. Sitar, and P. Günter, Vacuum **46**, 939 (1995).
[15]M. Barone *et al.* , J. Phys. Chem. C **126**, 3764 (2022).
[16]K. M. Adkison, S.-L. Shang, B. J. Bocklund, D. Klimm, D. G. Schlom, and Z.-K. Liu, APL Mater. **8**, 081110 (2020).
[17]D. Du, P. J. Strohbeen, H. Paik, C. Zhang, K. T. Genser, K. M. Rabe, P. M. Voyles, D. G. Schlom, and J. K. Kawasaki, J. Vac. Sci. Technol. B **38**, 022208 (2020).
[18]C. T. Parzyck *et al.*, Phys. Rev. Lett. **128**, 114801 (2022).
[19]H. Okamoto, J. Phase Equilib. **13**, 217 (1992).
[20]G. Koster, B. L. Kropman, G. J. Rijnders, D. H. Blank, and H. Rogalla, Appl. Phys. Lett. **73**, 2920 (1998).
[21]See the supplementary material at https://www.scitation.org/doi/suppl/10.1116/6.0002223 forFigs. S1–S9, a description of the flux calibration and $KTaO_3$ film growth and characterization.
[22]E. A. Zhurova, Y. Ivanov, V. Zavodnik, and V. Tsirelson, Acta Crystallogr., Sect. B: Struct. Sci. **56**, 594 (2000).
[23]R. Uecker, B. Velickov, D. Klimm, R. Bertram, M. Bernhagen, M. Rabe, M. Albrecht, R. Fornari, and D. Schlom, J. Cryst. Growth **310**, 2649 (2008).
[24]C. M. Culbertson, A. T. Flak, M. Yatskin, P. H.-Y. Cheong, D. P. Cann, and M. R. Dolgos, Sci. Rep. **10**, 3729 (2020).
[25]*Landolt-Börnstein: Numerical Data and Functional Relationships in Science and Technology*, edited by O. Madelung, Vol. 29a: Low frequency Properties of Dielectric Crystals (Springer-Verlag, Berlin, 1990), p. 96.
[26]R. Uecker, D. Klimm, R. Bertram, M. Bernhagen, I. Schulze-Jonack, M. Brützam, A. Kwasniewski, T. Gesing, and D. Schlom, Acta Phys. Pol., A **2**, 295 (2013).
[27]C. Brooks, L. F. Kourkoutis, T. Heeg, J. Schubert, D. Muller, and D. Schlom, Appl. Phys. Lett. **94**, 162905 (2009).
[28]B. Jalan, P. Moetakef, and S. Stemmer, Appl. Phys. Lett. **95**, 032906 (2009).
[29]R. C. Haislmaier, E. D. Grimley, M. D. Biegalski, J. M. LeBeau, S. Trolier-McKinstry, V. Gopalan, and R. Engel-Herbert, Adv. Funct. Mater. **26**, 7271 (2016).
[30]J. A. Moyer, C. Eaton, and R. Engel-Herbert, Adv. Mater. **25**, 3578 (2013).
[31]H.-T. Zhang, L. R. Dedon, L. W. Martin, and R. Engel-Herbert, Appl. Phys. Lett. **106**, 233102 (2015).
[32]M. Tyunina, J. Narkilahti, M. Plekh, R. Oja, R. M. Nieminen, A. Dejneka, and V. Trepakov, Phys. Rev. Lett. **104**, 227601 (2010).
[33]J. Thompson, J. Hwang, J. Nichols, J. G. Connell, S. Stemmer, and S. S. A. Seo, Appl. Phys. Lett. **105**, 102901 (2014).